Spectroscopic Analysis of Green, Desiccated and Dead Tamarisk Canopies

Ran Meng and Philip E. Dennison

Abstract

Defoliation by the northern tamarisk beetle (Diorhabda carinulata) causes changes in the reflectance of tamarisk (Tamarix spp.) canopies. Cross correlogram spectral matching was used to examine spectral separability of green, yellow desiccated, brown desiccated, and dead tamarisk canopy types. Using a feature selection technique (the instability index), four spectral regions were identified as important for canopy type discrimination, including one red (645-693 nm), one near infrared (735-946 nm), and two shortwave infrared regions (1,960-2,090 nm and 2,400-2,478 nm). The random forests decision tree algorithm was used to compare classification performances of full-range and feature-selected hyperspectral spectra as well as simulated WorldView-2 spectra. Classification results indicated that the process of feature selection can reduce data redundancy and computation time while improving accuracy of tamarisk canopy type classification.

Introduction

Tamarisk (*Tamarix* spp., a.k.a. saltcedar) is one of the most widely dispersed invasive plant species in the western United States, occupying an estimated 526,000 hectares and causing ecosystem service-related economic losses ranging between 133 and 285 million US dollars annually (Zavaleta, 2000), not to mention millions of dollars spent on eradication and restoration projects (Hultine *et al.*, 2010a). Previous studies have reported that tamarisk has cumulative negative effects on riparian ecosystems, such as reduced biodiversity, increased soil surface salinity, changes in riparian wildfire occurrence, and water use (Dudley *et al.*, 2000; Shafroth *et al.*, 2005). In order to control tamarisk, the northern tamarisk beetle (*Diorhabda carinulata*) has been released in the western United States (Tracy and Robbins, 2009). The beetle removes the leaf cuticle of tamarisk and eats the leaf mesophyll cells selectively in both the larval and adult stages, leading the leaf to desiccate and drop (Plate 1) (Meng *et al.*, 2012; Nagler *et al.*, 2014). Defoliation may not kill the tamarisk plant, and in many cases, tamarisk can refoliate in six to eight weeks after defoliation; however, studies show that the repeat defoliation caused by the tamarisk beetle can increase tamarisk mortality (Carruthers *et al.*, 2008; Dudley and Bean, 2012; Nagler *et al.*, 2014). Repeat herbivory caused up to 40 percent tamarisk mortality near the release sites after five years (Hultine *et al.*, 2010a).

Many studies have been implemented to investigate and monitor the impacts of beetle attack on tamarisk populations (Hudgeons *et al.*, 2007; Nagler *et al.*, 2008; Dennison *et al.*, 2009; Hultine *et al.*, 2010a; Hultine *et al.*, 2010b; Pattison *et al.*, 2011; Meng *et al.*, 2012; Nagler *et al.*, 2012; Snyder *et al.*, 2012; Nagler *et al.*, 2014). Due to the unexpected dispersal speed of the tamarisk beetle, the corresponding defoliation has spread to an extensive area that is unrealistic to track and analyze from the ground (Nagler *et al.*, 2014). Projected climate warming and drying trends in the southwestern United States may increase the over-winter survival of beetle populations, and consequently lead to increased herbivory (Dale *et al.*, 2001; Raffa *et al.*, 2008). Remote sensing techniques may be the most effective way to evaluate the effectiveness of tamarisk bio-control at the landscape scale (Dennison *et al.*, 2009; Meng *et al.*, 2012; Nagler *et al.*, 2012; Snyder *et al.*, 2012; Nagler *et al.*, 2014). Nevertheless, previous remote monitoring studies of tamarisk defoliation have not differentiated between desiccated (live) tamarisk canopies and dead tamarisk canopies at the stand scale (Dennison *et al.*, 2009; Meng *et al.*, 2012; Nagler *et al.*, 2012; Nagler *et al.*, 2014). Desiccated and dead tamarisk canopies will have very different ecosystem impacts, since desiccated canopies will regrow leaves and resume photosynthesis and transpiration. Identifying the spectral differences between green, desiccated and dead tamarisk canopies may help establish more informative and accurate assessment of tamarisk bio-control impacts and assist development of more adaptive management plans.

We hypothesized that spectral analysis techniques developed for hyperspectral processing can be used to study spectral features of tamarisk canopies and spectral separability among green, desiccated and dead tamarisk canopy spectra. If accurate classification of tamarisk canopy types based on field spectroscopy is proven feasible, hyperspectral and/or high spatial resolution imagery may be useful for mapping tamarisk bio-control impacts. The objectives of this study are to: (a) develop a methodology for selecting suitable wavelengths for discrimination of green, desiccated and dead tamarisk canopies, and (b) analyze the spectral signatures of these canopy types at both fine and coarse spectral resolutions.

Background

Previous studies of tamarisk defoliation by the northern tamarisk beetle have used multispectral remote sensing data from the Advanced Spaceborne Thermal Emission and Reflection Radiometer (ASTER), Landsat Thematic Mapper (TM), Landsat Enhanced Thematic Mapper+ (ETM+) and Moderate Resolution Imaging Spectroradiometer (MODIS) instruments. Dennison *et al.* (2009) mapped defoliation of large, dense tamarisk stands on the Colorado and Dolores Rivers using both ASTER and MODIS imagery. ASTER normalized difference vegetation index (NDVI) and MODIS enhanced vegetation index (EVI) both declined during periods of defoliation. Using Landsat TM imagery, Meng *et al.* (2012) compared two algorithms for

Department of Geography, University of Utah, 260 South Central Campus Dr., Room 270, Salt Lake City, UT 84112 (mengran07@gmail.com).

Photogrammetric Engineering & Remote Sensing
Vol. 81, No. 3, March 2015, pp. 199–207.
0099-1112/15/813–199

doi: 10.14358/PERS.81.3.199

detecting tamarisk defoliation, the forest disturbance index (Healey *et al.*, 2005) and a decision-tree model (random forests) (Breiman, 2001). Nagler *et al.* (2012) developed an approach for estimating regional evapotranspiration (ET) and foliage density changes caused by beetles using Landsat TM and MODIS data. Their results for six western US rivers indicated that defoliation events contributed to about 15 percent of the overall ET and foliage density reduction, with marked variations among river systems. Snyder *et al.* (2012) compared ET and carbon flux measured by eddy covariance to NDVI calculated from Landsat TM and ETM+ data. Declines in NDVI occurred during summer decreases in leaf area and ET caused by defoliation (Snyder *et al.*, 2012). Nagler *et al.* (2014) synthesized MODIS data, networked digital camera images and ground surveys to track beetle dispersal and its impacts on the Virgin River from 2010 to 2013. They concluded that beetle damage progressed at a rate of about 25 km yr^{-1}, much faster than previous expectations, and caused a 50 percent reduction in leaf area index and ET of tamarisk stands by 2012.

Identification of desiccated or dead tamarisk canopies may be aided by the availability of high spatial resolution (e.g., GeoEye, WorldView) or hyperspectral (e.g., Hyperion, AVIRIS) remote sensing data. High spatial resolution images may reduce spectral mixing at the stand scale to allow the separation of desiccated and dead canopies (Dennison *et al.* 2009, Meng *et al.* 2012), and can estimate ET at plant canopy scales (Nouri, 2014). In contrast with multispectral data, spectroscopic (hyperspectral) analysis can resolve spectral features related to vegetation structure and biochemistry using hundreds of near-contiguous narrow bandwidth channels (Ustin *et al.*, 2004). As a result, hyperspectral data have been used to assess spectral separability among different vegetation species (Dennison and Roberts, 2003; Pu, 2009; Van Aardt and Wynne, 2001), to estimate the change in biochemical compounds caused by disturbance or stress (Bian *et al.*, 2010; Estep and Carter, 2005; Pu *et al.*, 2008), and to distinguish between green plant, plant litter, and soil at both leaf and canopy levels (Nagler *et al.*, 2000; Nagler *et al.*, 2003; Inoue *et al.*, 2008). After measuring spectral reflectance of plant litter and soil samples using a spectroradiometer, Nagler *et al.* (2000 and 2003) found no unique spectral feature for discrimination of plant litter and soil existed in the visible or near infrared (NIR) spectral regions. However, in the shortwave infrared (SWIR) region, an absorption feature associated with cellulose and lignin was found and a corresponding spectral index called cellulose absorption index (CAI) was designed to quantify plant litter cover (Nagler *et al.*, 2000; Nagler *et al.*, 2003).

Various non-photosynthetic vegetation and green vegetation cover types have been successfully classified through spectral matching and linear mixture modeling techniques (Cochrane, 1998; Roberts *et al.*, 1998; Datt, 2000; Hostert *et al.*, 2003; Herold *et al.*, 2004; Daigo *et al.*, 2004; Zhang *et al.*, 2006; Sonnentag *et al.*, 2007; Zhang *et al.*, 2007; Pacheco and McNairn, 2010; Haest *et al.*, 2013; Somers and Asner, 2013). Spectral matching is one of the most widely used spectroscopic techniques, aiming to detect targeted pixels or endmembers, while linear spectral mixture analysis (LSMA) is designed for disaggregating mixed spectral pixels from remote sensing data sets. Asner and Lobell (2000) claimed that a careful selection of wavelengths or spectral features for LSMA may improve classification accuracy and reduce computation complexity. Somers *et al.* (2010) developed and tested an automated LSMA algorithm, known as stable zone unmixing (SZU), to overcome the limitations of the AutoSWIR algorithm presented by Asner and Lobell (2000). The instability index (ISI) was calculated to select stable spectral features (Somers *et al.*, 2008). ISI accounted for both the spectral variability within a class and the spectral similarity among classes to indicate the most useful and stable wavelength ranges over the full spectral range. Somers and Asner (2013) demonstrated that a proper wavelength selection strategy could avoid redundant information and improve classification accuracies, by emphasizing the subtle spectral and phenological differences among targeted classes. Discrimination of defoliated and dead tamarisk canopy types could benefit from a similar wavelength selection strategy.

Material and Methods

Study Site and Spectral Measurement

The study site was located at the University of Utah Rio Mesa Center, 65 km northeast of Moab in southeastern Utah. The riparian corridors along the Dolores River at Rio Mesa Center consist of dense tamarisk stands as well as some native cottonwood (*Populus fremontii*) and willow (*Salix gooddingii*) trees. As a first step towards spectroscopic analysis, the reflectance of green, desiccated and dead tamarisk canopies was measured *in situ* along the Dolores River over the 350-2,500 nm wavelength range using an Analytical Spectral Devices (ASD) field spectrometer with a 25° field of view (PANalytical; Analytic Spectral Devices, Boulder, Colorado). A white spectralon standard was used to calibrate the spectral measurements. The full-width-at-half maximum (FWHM) and the sampling interval of the spectrometer for the 350-1,050 nm spectral range were 3 nm and 1.4 nm, respectively. Over the 1,050-2,500 nm spectral range, the FWHM and sampling interval were 8 nm and 2 nm. A Gaussian function with a 5 nm FWHM was used to resample the 1 nm instrument output.

The reflectance measurements were carried out in early October 2013 within two hours before or after solar noon to reduce solar zenith angle effects, and under cloudless sky conditions. Reflectance spectra were measured from nadir at a height of approximately 15 cm above the canopy using a pistol grip with extension. The representative tamarisk canopy types (green, desiccated and dead) with different heights along riparian corridors were selected *in situ* to ensure significant variations in ground cover fractions and reflectance spectra. Desiccated tamarisk canopies showed two colors: yellow and brown (Plate 1). Dead canopies were devoid of desiccated leaf material, with only branches showing (Plate 1). Reflectance measurements for selected targets were performed five times and averaged for analysis. In total, 67 canopy spectra were collected and analyzed including 17 green, 15 dead, 27 yellow desiccated, and 8 brown desiccated canopies. Means and standard deviations for reflectance spectra of green, brown desiccated, yellow desiccated and dead canopies are shown in Figure 1. The major absorption regions influenced by atmospheric water vapor content were excluded from analysis (Somers *et al.*, 2009).

Cross Correlogram Spectral Matching

A suitable number of mapping classes is important for improving classification accuracy and efficiency (Richards and Jia, 2006). Desiccated tamarisk canopies showed two distinct colors (yellow and brown) *in situ* (Plate 1) representing different desiccated status, while Figure 1 indicated the spectral signatures of yellow and brown canopies were similar. Considering the computational task of remote sensing classification, it may be beneficial to examine if spectral separability between yellow and brown desiccated canopies is minor or if it is reasonable to split the desiccated canopy type into two subtypes (yellow and brown). A spectral matching technique called cross correlogram spectral matching (CCSM) was implemented to compare the spectral separability of different tamarisk canopy types (Van Der Meer and Bakker, 1997). CCSM compares the differences between a reference spectrum and an unknown spectrum in the form of reference amplitude as

Plate 1. Photographs of (a) green, (b) brown desiccated, (c)yellow desiccated, and (d) dead tamarisk canopies *in situ*.

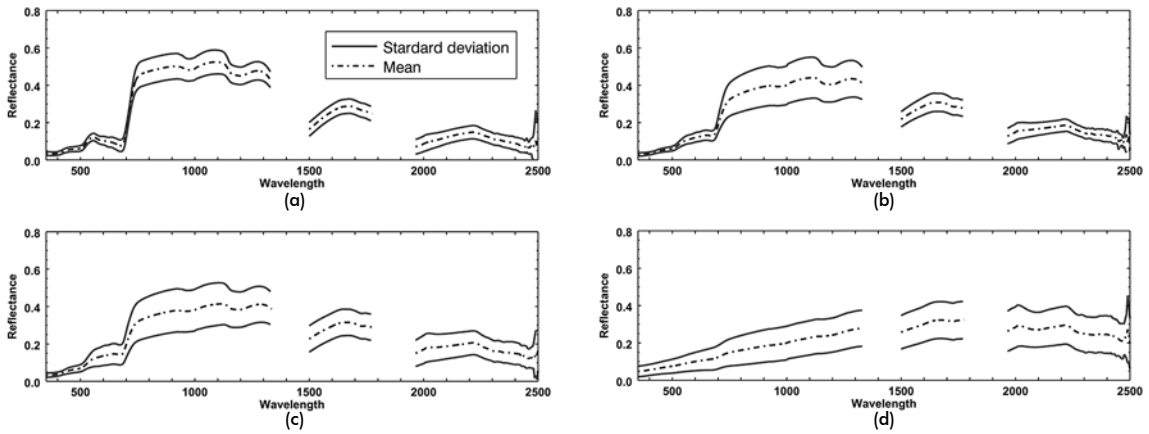

Figure 1. (a) Reflectance spectra of green, (b) brown desiccated, (c), yellow desiccated, and (d) dead tamarisk canopies. Atmospheric absorption regions were excluded.

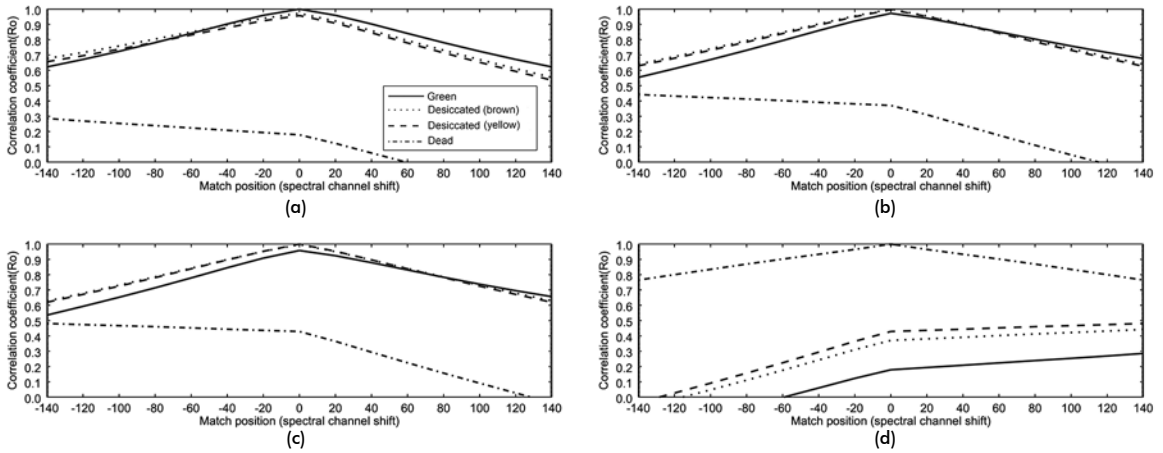

Figure 2. Cross correlograms using each tamarisk canopy type: (a) green, (b) brown desiccated, (c) yellow desiccated, and (d) dead as the reference over the 350-2,500 nm region.

well as shape variations. In the CCSM procedure, a reference spectrum is compared to a "test" spectrum by calculating the linear correlation coefficient between the two spectra at different match positions (Van Der Meer and Bakker, 1997; Datt, 2000). The cross correlogram function can be created by plotting the correlation coefficients against match positions. The location of the correlation maximum also indicates the degree of similarity between the test spectrum and the reference spectrum. The cross correlogram shape for high similarity is parabolic and symmetric around match position 0 with a peak correlation near to 1; on the contrary, the cross correlogram shape for low similarity is skewed with the correlation peak shifted towards either positive or negative match positions (Datt, 2000). Cross correlograms were calculated and inspected visually for different canopy type combinations (Figure 2), where "canopy type combination" refers to the comparison between a test spectrum (i.e., an averaged spectrum of samples from one tamarisk canopy type) and a reference spectrum (i.e., an averaged spectrum of samples from a second tamarisk canopy type) when applying CCSM.

The Instability Index

ISI was used to identify wavelengths that were least sensitive to spectral variability for tamarisk canopy classification (Somers *et al.*, 2008). ISI was calculated as the ratio of the within-class variability to the between-class variability (Somers et al., 2010):

$$\mathrm{ISI}_i = \frac{m}{m(m-1)} \sum_{z=1}^{m-1} \sum_{j=z+1}^{m} \frac{1.96(\delta_{z,i} + \delta_{j,i})}{\left| R_{z,i} - R_{j,i} \right|} \qquad (1)$$

where $R_{z,i}$ and $R_{j,i}$ are the reflectance values at wavelength i for class z and class, j, respectively, and $\delta_{z,i}$ and $\delta_{j,i}$ are the standard deviations at the same wavelengths of class z and j, respectively, and m is the number of classes. An ISI value that is below one indicates the between-class variability exceeds the within-class variability, while an ISI value which is above one signifies the opposite trend. Wavelengths with an ISI value below one are expected to contain useful information for spectral feature separation and should be selected for further analysis (Somers *et al.*, 2010).

Low ISI values were found for four spectral regions within the canopy spectra. Two of these spectral regions (red and NIR) corresponded to spectral regions covered by the high spatial resolution WorldView-2 multispectral instrument. WorldView-2 provides one panchromatic band (0.5 m spatial resolution) and eight multispectral bands (2 m spatial resolution) with an average revisit time of 1.1 days (Table1; *http://digitalglobe.com*). Considering the size and distribution of tamarisk stands along riparian corridors, WorldView-2 is one of the most suitable sensors for high spatial resolution remote monitoring of tamarisk defoliation and mortality, but lacks SWIR bands found on coarser spatial resolution sensors. Field-measured spectra were convolved using a sensor response function in ENVI software (*http://www.exelisvis.com/*) to simulate WorldView-2 multispectral spectra. ISI was also applied to select bands from the simulated WorldView-2 spectra. Following this convolution step, four sets of spectra were used for random forests classification analysis: full-range field spectra, feature-selected field spectra, simulated WorldView-2 spectra with all eight bands, and feature-selected WorldView-2 spectra with only bands 5 through 8 (Table 1).

Table 1. Wavelength Ranges of Multispectral Bands of the WorldView-2 Sensor (nm)

Band1 (coastal)	400-450	**Band5 (red)**	630-690
Band2 (blue)	450-510	**Band6 (red edge)**	705-745
Band3 (green)	510-580	**Band7 (NIR1)**	770-895
Band4 (yellow)	585-625	**Band8 (NIR2)**	860-1,040

Random Forests

The random forests (RF) algorithm was used to classify the tamarisk canopy field spectra and simulated WorldView-2 spectra. RF is a machine learning algorithm based on traditional decision tree classification. It randomly selects input variables from a large number of available variables and generates a large ensemble of independent tree classifiers that vote for class membership (Breiman, 2001). RF provides an internal unbiased estimate of the training set error called the out-of-bag (OOB) error (Breiman, 2001). During the process of RF classification, each tree classifier was constructed from bootstrapped samples comprising about two-thirds of the original dataset. Samples not used in the tree construction were put in the tree classifier to get a classification. In the end, a class is given to the largest number of votes from the OOB sample. The ratio of the times that a class is not the true class across all bootstrap iterations is called the OOB error estimation (Breiman, 2001). In addition, standard methods for evaluating classification accuracies such as confusion matrices and the kappa coefficient (Congalton, 1991a and 1991b; Congalton

Table 2. RF Confusion Matrices for Dead, Green, and Desiccated Canopies Using Full-Range and Feature-Selected Canopy Spectra

Full-range spectra	Dead canopies	Green canopies	Desiccated canopies	User's accuracy (%)
Dead canopies	12	0	3	80.0
Green canopies	0	12	5	70.6
Desiccated canopies	2	3	30	85.7
Producer's accuracy (%)	85.7	80.0	78.9	
OOB error (%), Kappa and run time (seconds)	17.9	0.678	1.37	
Feature-selected spectra				
Dead canopies	13	0	2	86.7
Green canopies	0	13	4	76.5
Desiccated canopies	2	3	30	85.7
Producer's accuracy (%)	86.7	81.3	83.3	
OOB error (%), Kappa and run time (seconds)	16.4	0.730	0.26	

Table 3. RF Confusion Matrices for Dead, Green, and Desiccated Canopies Using Simulated Full and Feature-Selected WorldView-2 Spectra

Full WV2 spectra	Dead canopies	Green canopies	Desiccated canopies	User's accuracy (%)
Dead canopies	13	0	2	86.7
Green canopies	0	13	4	76.5
Desiccated canopies	3	1	31	88.6
Producer's accuracy (%)	86.7	92.3	83.8	
OOB error (%), Kappa and run time (seconds)	14.93	0.753	0.08	
Feature-selected spectra				
Dead canopies	12	0	3	80.0
Green canopies	0	14	3	82.4
Desiccated canopies	2	1	32	91.4
Producer's accuracy (%)	85.7	93.3	84.2	
OOB error (%), Kappa and run time (seconds)	13.43	0.776	0.07	

and Green, 2009) were calculated to compare the RF classification of green, desiccated, and dead tamarisk canopies using full-range field spectra, feature-selected field spectra, 8-band simulated WorldView-2 spectra, and bands 5 through 8 from simulated WorldView-2 spectra.

Results

CCSM Results

Green, desiccated, and dead tamarisk canopy spectra had important differences in their reflectance spectra, but yellow desiccated and brown desiccated spectra were similar in terms of amplitude and shape (Figure 1). Mean green and desiccated canopy spectra possessed a steep increase in reflectance beyond visible wavelengths (>700 nm, referred to as the "red edge"), while the mean dead canopy spectrum showed a continual, gradual increase in reflectance. The contrast between the red and NIR spectral regions was highest for the mean green canopy spectrum, similar for both mean desiccated canopy spectra, and lowest for the mean dead canopy spectrum. The region with the highest reflectance (750-1,300 nm), called the "near infrared plateau," contains a unique plant spectral feature. Two liquid water absorption features were evident on the NIR plateau centered near 980 and 1,200 nm for both green and desiccated canopy spectra. The NIR plateau is produced by high internal leaf scattering at cell wall interfaces (Nilson and Olsson, 1995; Kokaly *et al.*, 2003). On the canopy level, NIR reflectance is further enhanced by multiple leaf layers which can amplify the already large difference in red and NIR reflectance of single leaves (Knipling, 1970). These spectral features are also influenced by proteins, lignin and cellulose (Kokaly *et al.*, 2003). Previous studies have indicated that the red and NIR regions can be used effectively for monitoring the active biomass of plant canopies and even vegetation vigor (Tucker, 1979, Rock *et al.*, 1988).

The SWIR spectral region has been identified as sensitive to vegetation moisture and senescence, and thus may be suitable for discrimination of green, desiccated and dead vegetation (Nagler *et al.*, 2000; Nagler *et al.*, 2003; Inoue *et al.*, 2008; Piekarczyk *et al.*, 2012). In the SWIR region, differences in amplitude can be observed among all the tamarisk canopy types (Figure 1), due to the changes in foliar water content (Gates *et al.*, 1965): the mean dead canopy spectrum had the highest reflectance value, the mean green canopy spectrum had the lowest, and the mean desiccated canopy spectra (brown and yellow) were in the middle but similar. The mean and ±1 standard deviation dead canopy spectra show evidence of lignin and cellulose absorption in the SWIR between 2,000 and 2,200 nm, while this spectral feature is not readily apparent in green or desiccated canopy spectra (Figure 1).

CCSM results were consistent with the visual assessment of reflectance spectra (Figure 2): in comparison to other canopy type combinations, spectra of yellow and brown desiccated canopies were very similar with little difference, and the dead canopy spectrum was significantly different from the spectra of other canopy types. The cross correlogram with the reference spectrum itself was parabolic and nearly symmetrical with a correlation maximum up to 1 at match position 0, indicating a perfect match. Canopy type combinations using the green, yellow desiccated, and brown desiccated canopy spectra as reference spectra showed that the dead canopy spectrum was distinct. The dead canopy cross correlograms were highly skewed with much smaller correlation coefficients, and the correlation peak was shifted towards positive match positions (Figure 2). The cross correlograms for yellow/brown desiccated canopy

and green canopy combinations were moderately skewed, but the correlation maxima were still high around match position 0; most important of all, the cross correlograms of yellow and brown desiccated canopies combinations were mostly indistinguishable. Since the differences between yellow and brown desiccated canopies were proven to be small and hard to distinguish, these canopy types were combined into a single desiccated canopy type for further analysis.

Feature-selected Wavelengths

Figure 3 plots ISI values based on the reflectance of green, desiccated and dead canopy spectra as a function of wavelength. As previously explained in the Instability Index Section, low ISI values were expected to correspond with low levels of similarity between canopy types and/or low levels of variability within each canopy type indicating high separability. In the end, the feature-selected wavelengths with low ISI values were found in four spectral regions: one red region (645-693 nm), one NIR region (735-946 nm), and two SWIR regions (1,960-2,090 nm and 2,400-2,478 nm). In previous studies, these regions were sensitive to changes in chlorophyll, damaged leaf layer structures and loss of water content (Knipling, 1970; Heller, 1978; Boochs *et al.*, 1990; Carter, 1993; Radeloff *et al.*, 1999; Lentile *et al.*, 2006; Inoue *et al.*, 2008; Piekarczyk *et al.*, 2012).

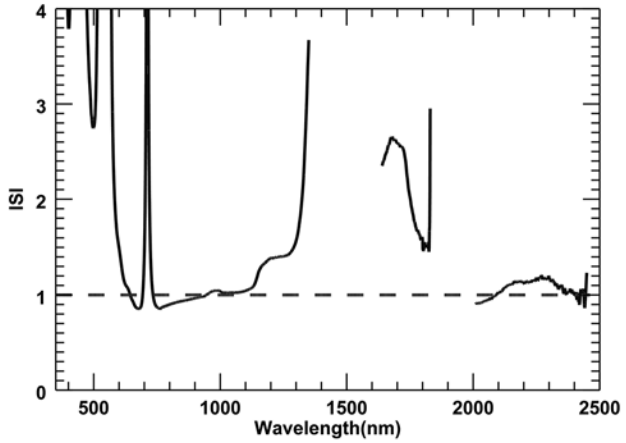

Figure 3. ISI values based on the reflectance of green, desiccated, and dead canopy spectra, plotted against wavelength. Atmosphere absorption regions were excluded.

Classification of Full-range and Feature-selected Spectra

RF confusion matrices, OOB error, kappa, and run time were used to compare the classification performance of full-range and feature-selected spectra (Table 2 and Table 3). In general, desiccated canopies were the most difficult to distinguish and caused most of the classification errors among the three canopy types. User's accuracy for green canopies was lowest (70.6 percent) using the full-range spectra, due to the misclassifications of green and desiccated canopies. In addition, Table 2 showed that using the feature-selected spectra instead of the full-range spectra, the OBB error dropped from 17.9 percent to 16.4 percent. Correspondingly, the kappa coefficients of confusion matrices increased from 0.678 to 0.730. The computation time of feature-selected spectra decreased significantly compared to full-range spectra. Using a desktop computer, the run time of RF classification for feature-selected spectra was 0.26 seconds, while the time for full range spectra was 1.37 seconds.

In comparison with the full WorldView-2 spectra, the feature-selected set of WorldView-2 spectra tended to have higher accuracy or lower OOB error (Table 3). These results indicate that a process of feature selection is likely beneficial for improving classification accuracy and reducing the computation time. Kappa values indicate that separation of canopy types improved when WorldView-2 bands were used, indicating that classification of green, desiccated, and dead tamarisk canopies may not require SWIR bands or hyperspectral data.

Based on high accuracies for feature-selected canopy and simulated WorldView-2 spectra, the same feature-selected bands were applied to classification of four classes: green canopy, yellow desiccated canopy, brown desiccated canopy, and dead canopy. Table 4 shows the classification performance for using feature-selected canopy spectra for separation of desiccated yellow and desiccated brown classes. User's accuracy for brown desiccated canopies was 0 percent, due to the misclassification error between yellow and brown desiccated canopy spectra. In comparison to the classification performance based on three canopy types (Table 2), OOB error increased to 32.84 percent from 16.4 percent and kappa coefficient decreased to 0.526 from 0.730 (Table 4). Using the best classification for three canopy types (four-band WorldView-2 spectra), classification for four classes was attempted again. OOB increased from 13.43 percent to 28.36 percent, and at the same time, kappa coefficient decreased dramatically from 0.776 to 0.585 (Table 3, Table 5). Similar to the results from CCSM, Table 4 and Table 5 indicate that combining desiccated canopies into one type was necessary.

Discussion and Conclusions

Our study contributes to continuing efforts for evaluating the impacts of tamarisk bio-control in the western United States, and extends our understanding of vegetation disturbance monitoring. Compared to previous studies using high spatial resolution or hyperspectral imagery to map vegetation canopy disturbance, our analysis using field spectra had similar classification accuracy. Using high spatial resolution (<4 m) QuickBird-2 images, Wulder *et al.* (2008) mapped mountain pine beetle "red attack" with 89 percent to 93 percent accuracies in British Columbia, Canada. Based on airborne hyperspectral imagery (PROSPECTIR-VS, 2 m spatial resolution) and field measurements, Santos *et al.* (2010) mapped asymptomatic, senesced and dead trees in a pine forest of southeastern United States using a decision tree method. Stressed tree mapping had a kappa coefficient of around 0.70, indicating that asymptomatic trees are likely to have significantly higher reflectance in the red-NIR regions, senescent trees are likely to have significantly lower reflectance in the NIR regions, and dead trees are likely to have significantly higher reflectance in the SWIR regions.

Our analysis applied wavelength selection techniques on canopy spectra collected *in situ* before classification by RF, resulting in an increased classification accuracy of tamarisk canopy types compared to using the full wavelength range (Asner *et al.*, 1998; Somers *et al.*, 2010; Somers and Asner, 2013). Using selected wavelengths (bands) that display high between-class variability and low within-class variability, not only was higher classification accuracy achieved, but the computational time was greatly reduced (Table 2 and Table 3). In addition, feature-selected WorldView-2 bands demonstrated better classification performances over field spectra for separating green, desiccated, and dead canopy types. Somers and Asner (2013) hypothesized that redundant spectral information in hyperspectral data caused decreased accuracy and additional computational time in the spectral mixture analysis. Redundant spectral information may have caused lower classification accuracies for full spectrum canopy spectra and simulated WorldView-2 spectra used in this study.

In conclusion, this study proposed a methodology to improve remote monitoring of tamarisk bio-control by a combination of spectral analysis techniques (CCSM, ISI, and

Table 4. RF Confusion Matrices for Dead, Green, Yellow, and Brown Canopies Using Feature-Selected Canopy Spectra

	Dead canopies	Brown canopies	Green canopies	Yellow canopies	User's accuracy (%)
Dead canopies	14	0	0	1	93.3
Brown canopies	0	0	0	8	0.0
Green canopies	0	0	13	4	76.5
Yellow canopies	2	4	3	18	66.7
Producer's accuracy (%)	87.5	0.0	81.3	58.0	
OOB error (%), Kappa and run time (seconds)	32.84	0.526	0.74		

Table 5. RF Confusion Matrices for Dead, Green, Yellow, and Brown Canopies Using Simulated Feature-Selected WorldView-2 Spectra

	Dead canopies	Brown canopies	Green canopies	Yellow canopies	User's accuracy (%)
Dead canopies	12	0	0	3	80.0
Brown canopies	0	1	0	7	12.5
Green canopies	0	0	14	3	82.4
Yellow canopies	2	2	2	21	77.8
Producer's accuracy (%)	85.7	33.3	87.5	61.8	
OOB error (%), Kappa and run time (seconds)	28.36	0.585	0.07		

RF). The step of feature selection might be useful not only for spectral mixture analysis of hyperspectral remote sensing, but also for multi-spectral remote sensing classifications. The red, NIR, and SWIR wavelength regions were found to be important for discriminating desiccated and dead canopy spectra. Our analysis shows again that the variations in spectral signatures caused by stress or disturbance are not equal across the full wavelength range, and that spectral features at specific wavelengths are valuable for monitoring disturbed or stressed plant canopies (Ahern *et al.*, 1991; Radeloff *et al.*, 1999; Hurley *et al.*, 2004; Santos *et al.*, 2010).

Further studies evaluating the impacts of the tamarisk biocontrol program could be accomplished using data acquired from high spatial resolution sensors (i.e., WorldView-2) and ground-based ET measurements. More detailed and accurate mapping of tamarisk canopy classes may be possible with high spatial resolution, multispectral data. By exploring the relationship between spectral indices and ground-based ET measurements, high spatial resolution data may also assist in assessing water salvage (Nouri, 2014). Multi-temporal analysis using either high spatial resolution multispectral or hyperspectral data may also result in improved classification of tamarisk defoliation and mortality, as well as identification of mortality trends over time.

Acknowledgments

The authors would like to thank the Donald R. Currey Graduate Research Scholarship and University of Utah Rio Mesa Center for supporting the Dolores River field work. We also would like to thank following people for their valuable contributions to the Dolores River field work: Zachary Lundeen, Hau Truong, Kenneth Dudley, and Timothy Edgar.

References

Ahern, F.J., T. Erdle, D.A. Maclean, I.D. Kneppeck, 1991. A quantitative relationship between forest growth rates and Thematic Mapper reflectance measurements, *International Journal of Remote Sensing*, 12:387–400.

Asner, G.P., and D.B. Lobell, 2000. A biogeophysical approach for automated SWIR unmixing of soils and vegetation, *Remote Sensing of Environment*, 74:99–112.

Asner, G.P., C.A. Wessman, D.S. Schimel, and S. Archer,1998. Variability in leaf and litter optical properties: Implications for BRDF model inversions using AVHRR, MODIS, and MISR, *Remote Sensing of Environment*, 63:243–257.

Bian, M., A.K. Skidmore, M. Schlerf, T. Fei, Y. Liu, and T. Wang, 2010. Reflectance spectroscopy of biochemical components as indicators of tea (*Camellia sinensis*) quality, *Photogrammetric Engineering & Remote Sensing*, 76(12):1385–1392.

Boochs, F., G. Kupfer, K. Dockter, and W. Kuêhbauch, 1990. Shape of the red edge as vitality indicator for plants, *International Journal of Remote Sensing*, 11:1741–1753.

Breiman, L., 2001. Random forests, *Machine Learning*, 45:5–32.

Carruthers, R.I., C.J. DeLoach, J.C. Herr, G.L. Anderson, and A.E. Knutson, 2008. Areawide pest management: Theory and implementation, *Salt Cedar Areawide Pest Management in the Western USA* (O. Koul, editor), CAB International, Wallingford, UK, pp. 271–299.

Carter, G.A., 1993. Responses of leaf spectral reflectance to plant stress, *American Journal of Botany*, 80:239–243.

Cochrane, M.A., 1998. Linear mixture model classification of burned forests in the Eastern Amazon, *International Journal of Remote Sensing*, 19:3433–3440.

Congalton, R.G., 1991a. A review of assessing the accuracy of classifications of remotely sensed data, *Remote Sensing of Environment*, 37:35–46.

Congalton, R.G., 1991b. Remote sensing and geographic information system data integration: error sources and, *Photogrammetric Engineering & Remote Sensing*, 57(5):677–687.

Congalton, R.G., and K. Green, 2009. *Assessing the Accuracy of Remotely Sensed Data: Principles and Practices*, Second edition, CRC/Taylor & Francis, Boca Raton, Florida, 150 p.

Daigo, M., A. Ono, R., Urabe, and N. Fujiwara, 2004. Pattern decomposition method for hyper-

multi-spectral data analysis, *International Journal of Remote Sensing*, 25:1153–1166.

Dale, V.H., L.A. Joyce, S. McNulty, R.P. Neilson, M.P. Ayres, M.D. Flannigan, P.J. Hanson, L.C. Irland, A.E. Lugo, C.J. Peterson, F.J. Swanson, B.J. Stocks, and B.M Wotton, 2001. Climate change and forest disturbances, *BioScience*, 51:723–734.

Datt, B., 2000. Identification of green and dry vegetation components with a cross-correlogram spectral matching technique, *International Journal of Remote Sensing*, 21:2133–2139.

Dennison, P.E., and D.A. Roberts, 2003. Endmember selection for multiple endmember spectral mixture analysis using endmember average RMSE, *Remote Sensing of Environment*, 87:123–135.

Dennison, P.E.,P.L. Nagler, K.R. Hultine, E.P. Glenn, and J.R. Ehleringer, 2009. Remote monitoring of tamarisk defoliation and evapotranspiration following saltcedar leaf beetle attack, *Remote Sensing of Environment*, 113:1462–1472.

Dudley, T.L., and D.W. Bean, 2012. Tamarisk biocontrol, endangered species risk and resolution of conflict through riparian restoration, *BioControl*, 57:331–347.

Dudley, T. L., C.J. DeLoach, L.E. Lovich, and R.I. Carruthers, 2000. Saltcedar invasion of western riparian areas: Impacts and new prospects for control, *Transactions of the 65th North American Wildlife & Natural Resources Conference*,24-28 March 2000, Wildlife Management Institute, Washington, D.C., Chicago, Illoinos, pp. 345–381.

Estep, L., and G.A. Carter, 2005. Derivative analysis of AVIRIS data for crop stress detection, *Photogrammetric Engineering & Remote Sensing*, 71(12):1417–1421.

Gates, D. M., H.J. Keegan, J.C. Schleter, and V.R. Weidner 1965. Spectral Properties of Plants, *Applied Optics*, 4:11–20.

Haest, M., T. Cudahy, A. Rodger, C. Laukamp, E. Martens, and M. Caccetta, 2013. Unmixing the effects of vegetation in airborne hyperspectral mineral maps over the Rocklea Dome iron-rich palaeochannel system (Western Australia), *Remote Sensing of Environment*, 129:17–31.

Healey, S. P., W.B. Cohen, Y. Zhiqiang, and O.N. Krankina, 2005. Comparison of Tasseled Cap-based Landsat data structures for use in forest disturbance detection, *Remote Sensing of Environment*, 97:301–310.

Heller, R.C., 1978. Case applications of remote sensing for vegetation damage assessment, *Photogrammetric Engineering & Remote Sensing*, 44(10):1159–1166.

Herold, M., D.A. Roberts, M.E. Gardner, and P.E. Dennison, 2004. Spectrometry for urban area remote sensing - Development and analysis of a spectral library from 350 to 2400 nm, *Remote Sensing of Environment*, 91:304–319.

Hostert, P., A. Röder, and J. Hill, 2003. Coupling spectral unmixing and trend analysis for monitoring of long-term vegetation dynamics in Mediterranean rangelands, *Remote Sensing of Environment*, 87:183–197.

Hudgeons, J.L., A.E. Knutson, K.M. Heinz, C.J. DeLoach, T.L. Dudley, R.R. Pattison, and J.R. Kiniry, 2007. Defoliation by introduced *Diorhabda elongata* leaf beetles (Coleoptera: Chrysomelidae) reduces carbohydrate reserves and regrowth of *Tamarix* (Tamaricaceae), *Biological Control*, 43:213–221.

Hultine, K.R.,J. Belnap, P. Dennison, J. Ehleringer, M. Lee, P. Nagler, K. Snyder, S. Snyder, S. Uselman, C. Van Riper, and J. Weeks, 2010a. Tamarisk biocontrol in the western United States: Ecological and societal implications, *Frontiers in Ecology and the Environment*, 8:467-474.

Hultine, K.R., P.L. Nagler, K. Morino, S.E. Bush, K.G. Burtch, P.E. Dennison, E.P. Glenn, and J.R. Ehleringer, 2010b. Sap flux-scaled transpiration by tamarisk (*Tamarix* spp.) before, during and after episodic defoliation by the saltcedar leaf beetle (*Diorhabda carinulata*), *Agricultural and Forest Meteorology*, 150:1467–1475.

Hurley, A., D. Watts, B. Burke, and C. Richards, 2004. Identifying gypsy moth defoliation in Ohio using Landsat data, *Environmental & Engineering Geoscience*, 10:321–328.

Inoue, Y., J. Qi, A. Olioso, Y. Kiyono, T. Horie, H. Asai, K. Saito, Y. Ochiai, T. Shiraiwa, and L. Douangsavanh, 2008. Reflectance characteristics of major land surfaces in slash and burn ecosystems in Laos, *International Journal of Remote Sensing*, 29:2011–2019.

Knipling, E.B., 1970. Physical and physiological basis for the reflectance of visible and near-infrared radiation from vegetation, *Remote Sensing of Environment*, 1:155–159.

Kokaly, R.F., D.G.Despain, R.N. Clark, and K.E. Livo, 2003. Mapping vegetation in Yellowstone National Park using spectral feature analysis of AVIRIS data, *Remote Sensing of Environment*, 84:437–456.

Lentile, L.B.,Z.A. Holden, A.M.S. Smith, M.J. Falkowski, A.T. Hudak, P. Morgan, S.A. Lewis, P.E. Gessler, and N.C. Bensen, 2006. Remote sensing techniques to assess active fire characteristics and post-fire effects, *International Journal of Wildland Fire*, 15:319–345.

Meng, R., P.E. Dennison, L.R. Jamison, C. van Riper III, P. Nager, K.R. Hultine, D.W. Bean, and T. Dudley, 2012. Detection of tamarisk defoliation by the northern tamarisk beetle based on multitemporal Landsat 5 Thematic Mapper imagery, *GIScience & Remote Sensing*, 49:510–537.

Nagler, P.L., C.S.T. Daughtry, and S.N. Goward, 2000. Plant litter and soil reflectance, *Remote Sensing of Environment*, 71:207–215.

Nagler, P.L., Y. Inoue, E.P. Glenn, A.L. Russ, and C.S.T. Daughtry, 2003. Cellulose absorption index (CAI) to quantify mixed soil-plant litter scenes, *Remote Sensing of Environment*, 87:310–325.

Nagler, P.L., T. Brown, K.R. Hultine, C. van Riper III, D.W. Bean, P.E. Dennison, R.S. Murray, and E.P. Glenn, 2012. Regional scale impacts of Tamarix leaf beetles (*Diorhabda carinulata*) on the water availability of western U.S. rivers as determined by multi-scale remote sensing methods, *Remote Sensing of Environment*, 118:227–240.

Nagler, P. L., E.P. Glenn, K. Didan, J. Osterberg, F. Jordan, and J. Cunningham, 2008. Wide area estimates of stand structure and water use of *Tamarix* spp. on the lower Colorado River: Implications for restoration and water management projects, *Restoration Ecology*, 16:136–145.

Nagler, P.L., E.P. Glenn, K. Didan, J. Osterberg, F. Jordan, and J. Cunningham, 2014. Rapid dispersal of saltcedar (*Tamarix* spp.) biocontrol beetles (*Diorhabda carinulata*) on a desert river detected by phenocams, MODIS imagery and ground observations, *Remote Sensing of Environment*, 140:206–219.

Nilson, T., and H. Olsson, 1995. Effect of thinning cutting on boreal forest reflectance: A comparison of simulations and Landsat TM estimates, *International Journal of Remote Sensing*, 16:2963–2968.

Nouri, H., S. Beecham, S. Anderson, and P. Nagler, 2014. High spatial resolution WorldView-2 imagery for mapping NDVI and its relationship to temporal urban landscape evapotranspiration factors, *Remote Sensing*, 6:580–602.

Pacheco, A., and H. McNairn, 2010. Evaluating multispectral remote sensing and spectral unmixing analysis for crop residue mapping, *Remote Sensing of Environment*, 114:2219–2228.

Pattison, R.R.,C.M. D'Antonio, and T.L. Dudley, 2011. Biological control reduces growth, and alters water relations of the saltcedar tree (*Tamarix* spp.) in western Nevada, USA, *Journal of Arid Environments*, 75:346–352.

Piekarczyk, J., C. Kaömierowski, and S. Królewicz, 2012. Relationships between soil properties of the abandoned fields and spectral data derived from the advanced spaceborne thermal emission and reflection radiometer (ASTER), *Advances in Space Research*, 49:280–291.

Pu, R., 2009. Broadleaf species recognition with *in situ* hyperspectral data, *International Journal of Remote Sensing*, 30:2759–2779.

Pu, R., M. Kelly, G.L. Anderson, and P. Gong, 2008. Using CASI hyperspectral imagery to detect mortality and vegetation stress associated with a new hardwood forest disease, *Photogrammetric Engineering & Remote Sensing*, 74(5):65–75.

Radeloff, V.C., D.J. Mladenoff, and M.S. Boyce, 1999. Detecting Jack Pine budworm defoliation using spectral mixture analysis: Separating effects from determinants, *Remote Sensing of Environment*, 69:156–169.

Raffa, K.F., B.H. Aukema, B.J. Benz, A.L. Calloll, J.A. Hicke, M.G Turner, and W.H. Romme, 2008. Cross-scale drivers of natural disturbances prone to anthropogenic amplification: The dynamics of bark beetle eruptions, *Bioscience*, 58:501–517.

Richards, J.A.,and X. Jia, 2006. *Remote Sensing Digital Image Analysis*, Springer, Berlin, Germany, 439 p.

Roberts, D.A., M. Gardener, R. Church, S. Ustin, G. Scheer, and R.O. Green, 1998. Mapping chaparral in the Santa Monica Mountains using multiple endmember spectral mixture models, *Remote Sensing of Environment*, 65:267–279.

Rock, B.N., B.N. Rock, T. Hoshizaki, and J.R. Miller, 1988. Comparison of *in situ* and airborne spectral measurements of the blue shift associated with forest decline, *Remote Sensing of Environment*, 24:109–127.

Santos, M.J., J.A. Greenberg, and S.L. Ustin, 2010. Using hyperspectral remote sensing to detect and quantify southeastern pine senescence effects in red-cockaded woodpecker (*Picoides borealis*) habitat, *Remote Sensing of Environment*, 114:1242–1250.

Shafroth, P.B., J.R. Cleverly, T.L. Dudley, J.P. Taylor, C. Van Riper III, E.P. Weeks, and J.N. Stuart, 2005. Control of *Tamarix* in the western United States: implications for water salvage, wildlife use, and riparian restoration, *Environmental Management*, 35:231–246.

Snyder, K.A., R.L. Scott, and K., McGwire, 2012. Multiple year effects of a biological control agent (*Diorhabda carinulata*) on *Tamarix* (saltcedar) ecosystem exchanges of carbon dioxide and water, *Agricultural and Forest Meteorology*, 164:161–169.

Somers, B., and G.P. Asner, 2013. Multi-temporal hyperspectral mixture analysis and feature selection for invasive species mapping in rainforests, *Remote Sensing of Environment*, 136:14–27.

Somers, B., K. Cools, S. Delalieux, J. Stuckens, D. Van der Zande, W.W. Verstraeten, and P. Coppin, 2009. Nonlinear hyperspectral mixture analysis for tree cover estimates in orchards, *Remote Sensing of Environment*, 113: 1183–1193.

Somers, B., K. Cools, S. Delalieux, J. Stuckens, D. Van der Zande, W.W. Verstraeten, and P. Coppin, 2008. A weighted linear spectral mixture analysis approach to address endmember variability in agricultural production systems, *International Journal of Remote Sensing*, 30:139–147.

Somers, B., K. Cools, S. Delalieux, J. Stuckens, D. Van der Zande, W.W. Verstraeten, and P. Coppin,2010. An automated waveband selection technique for optimized hyperspectral mixture analysis, *International Journal of Remote Sensing*, 31:5549–5568.

Sonnentag, O., J.M. Chen, D.A. Roberts, J. Talbot, K.Q. Halligan, and A. Govind, 2007. Mapping tree and shrub leaf area indices in an ombrotrophic peatland through multiple endmember spectral unmixing, *Remote Sensing of Environment*, 109:342–360.

Tracy, J.L., and T.O. Robbins, 2009. *Taxonomic Revision and Biogeography of the Tamarix-Feeding Diorhabda elongata (Brullé, 1832) Species Group (Coleoptera: Chrysomelidae: Galerucinae: Galerucini) and Analysis of Their Potential in Biological Control of Tamarisk*, Magnolia Press, Auckland, New Zealand, 152 p.

Tucker, C.J., 1979. Red and photographic infrared linear combinations for monitoring vegetation, *Remote Sensing of Environment*, 8:127–150.

Ustin, S.L., D.A. Roberts, J.A. Gamon, G.P. Asner, and R.O. Green, 2004. Using imaging spectroscopy to study ecosystem processes and properties, *BioScience*, 54:523–534.

Van Aardt, J.A.N., and R.H. Wynne, 2001. Spectral separability among six southern tree species, *Photogrammetric Engineering & Remote Sensing*, 67(12):1367–1375.

Van Der Meer, F., and W. Bakker, 1997. CCSM: Cross correlogram spectral matching, *International Journal of Remote Sensing*, 18:1197–1201.

Wulder, M.A., J.C. White, N.C., Coops, and C.R. Butson, 2008. Multitemporal analysis of high spatial resolution imagery for disturbance monitoring, *Remote Sensing of Environment*, 112:2729–2740.

Zavaleta, E., 2000. The economic value of controlling an invasive shrub, *Ambio*, 29:462–467.

Zhang, L., S. Furumi, K., Muramatsu, N. Fujiwara, M. Daigo, and L. Zhang, 2006. Sensor independent analysis method for hyperspectral data based on the pattern decomposition method, *International Journal of Remote Sensing*, 27:4899–4910.

Zhang, L.,S. Furumi, K. Muramatsu, N. Fujiwara, M. Daigo, and L. Zhang, 2007. A new vegetation index based on the universal pattern decomposition method, *International Journal of Remote Sensing*, 28:107–124.

(Received 26 April 2014; accepter 04 August 2014; final version 13 October 2014)